Available online at www.sciencedirect.com

ScienceDirect

Nuclear and Particle Physics Proceedings 273–275 (2016) 901–906

www.elsevier.com/locate/nppp

Higgs Boson Decays to Leptons with the ATLAS Detector

Elias Coniavitis*

Albert-Ludwigs-Universität Freiburg
elias.coniavitis@cern.ch

Abstract

A review of the results on Higgs boson decays to leptons with the ATLAS detector at the Large Hadron Collider is presented. In the $H \to \tau^+\tau^-$ search, using the 8 TeV dataset, there is an excess of data over the background prediction, with an observed (expected) significance corresponding to 4.1σ (3.2σ). In the $H \to \mu^+\mu^-$ search, using approximately 25 fb^{-1} of pp collision data collected at 7 TeV and 8 TeV in 2011 and 2012, the data is consistent with the expected background and a 95% confidence level limit of 7.0 times the Standard Model prediction is placed on the signal strength, for a Higgs boson mass of 125.5 GeV.

Keywords: Higgs boson, leptons, ATLAS

1. Introduction

The observation by the ATLAS and CMS collaborations of a new particle with a mass around 125 GeV [1, 2] is a very significant success of the Large Hadron Collider [3] physics program. The signal strength of the new particle as well as measurements of its properties [4–7] are all consistent with the predictions for the Standard Model (SM) Higgs boson [8–13]. These measurements however rely primarily on the bosonic decays of the Higgs boson, $H \to \gamma\gamma$, $H \to ZZ^*$ and $H \to WW^*$. To confirm or reject its SM nature, and understand the mass generation mechanism for fermions, it therefore remains very important to demonstrate and measure the direct coupling of the Higgs boson to fermions and investigate its proportionality to mass.

This note presents the results of searches with the ATLAS detector [14] for Higgs boson decays to leptons: $H \to \tau^+\tau^-$ [15] and $H \to \mu^+\mu^-$ [16]. $H \to \tau^+\tau^-$ has the largest branching ratio of all SM Higgs boson decays to leptons (6.24×10^{-2})[1] but leads to a challenging final state and a poor mass resolution, while $H \to \mu^+\mu^-$ on the other hand has a good mass resolution but a much lower branching ratio (2.16×10^{-4})[1] [17].

2. Higgs boson decays to tau leptons

The $H \to \tau^+\tau^-$ decay is the most sensitive channel for leptonic Higgs boson decays, due to its high branching ratio, although the fact that the τ lepton decays inside the detector to final states involving neutrinos complicates the experimental signature and substantially worsens the mass resolution. In order to maximize the sensitivity, a multivariate analysis based on Boosted Decision Trees (BDT) [18–20] is performed, and the full 8 TeV dataset collected by the ATLAS detector is used.

2.1. Analysis Description

All decays of the τ lepton (both leptonic, τ_{lep}, and hadronic, τ_{had}) are considered, leading to three sub-channels denoted $\tau_{\text{lep}}\tau_{\text{lep}}$, $\tau_{\text{lep}}\tau_{\text{had}}$ and $\tau_{\text{had}}\tau_{\text{had}}$. The three sub-channels are defined by orthogonal cuts on the number of reconstructed hadronic τ decays and *light* leptons (electrons or muons). Following a preselection, detailed in [15], events in each sub-channel

*On behalf of the ATLAS Collaboration

[1] For a Higgs boson mass of $m_H = 125.5$ GeV.

http://dx.doi.org/10.1016/j.nuclphysbps.2015.09.139

are split into two categories. The *VBF Category* contains events with two jets separated in pseudo-rapidity and targets signal events produced through Vector Boson Fusion (VBF). The *Boosted Category* targets signal events where the Higgs boson has been produced with a large boost, primarily from the gluon fusion process (ggF), and requires the transverse momentum (p_{T}) of the reconstructed Higgs boson candidate to be greater than 100 GeV. Table 1 details the categorization criteria in each sub-channel.

Selection	$\tau_{\mathrm{lep}}\tau_{\mathrm{lep}}$	$\tau_{\mathrm{lep}}\tau_{\mathrm{had}}$	$\tau_{\mathrm{had}}\tau_{\mathrm{had}}$
VBF Category			
$p_{\mathrm{T}}(j_1) >$	40	50	50
$p_{\mathrm{T}}(j_2) >$	30	30	30/35
$\Delta\eta(j_1, j_2) >$	2.2	3.0	2.0
b-jet veto for jet $p_{\mathrm{T}} >$	25	30	-
$p_{\mathrm{T}}^{H} >$	-	-	40
Boosted Category			
$p_{\mathrm{T}}(j_1) >$	40	-	-
$p_{\mathrm{T}}^{H} >$	100	100	100
b-jet veto for jet $p_{\mathrm{T}} >$	25	30	-

Table 1: Categorization criteria applied for each sub-channel of the $H \to \tau^+\tau^-$ search. All p_{T} threshold values are in GeV, while j_1 and j_2 represent the most energetic and the second most energetic jet in the event. Only events failing the VBF category selection are considered for the Boosted category, to ensure orthogonality. Events in the $\tau_{\mathrm{lep}}\tau_{\mathrm{had}}$ VBF category must additionally satisfy $m_{\ell,\tau_h} > 40$ GeV. The $\tau_{\mathrm{had}}\tau_{\mathrm{had}}$ $p_{\mathrm{T}}(j_2)$ threshold is 30(35) GeV for jets within (outside of) $|\eta| < 2.4$.

This leads to six Signal Regions (category and sub-channel combinations), and separate BDTs are trained for each, using between six and nine input variables. The selection of these variables has been separately optimized for each signal region, and chosen in order to exploit discriminating features such as resonance properties, event activity and topology, as well as the characteristic VBF topology in the corresponding category. One of the most important input variables is the mass of the di-τ system, the reconstruction of which is quite challenging due to the presence of at least two neutrinos in the final state; the Missing Mass Calculator (MMC) is used for this purpose [21]. Figure 1 shows a comparison of reconstructed masses for the data-based estimation of $Z \to \tau^+\tau^-$ (see next paragraph) and signal Monte Carlo in the $\tau_{\mathrm{lep}}\tau_{\mathrm{lep}}$ channel, which has four neutrinos in the final state.

The background composition differs between each sub-channel, but in all three the most important backgrounds are irreducible $Z \to \tau^+\tau^-$ events, and backgrounds with a jet misidentified as a τ decay product. To

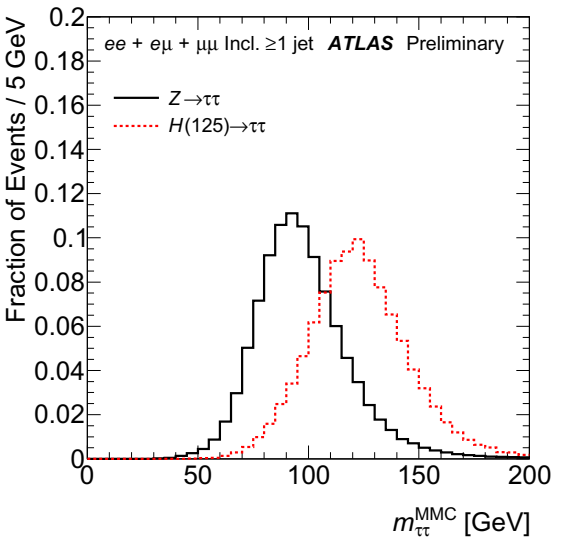

Figure 1: Reconstructed mass of the di-τ system using the MMC algorithm in the $\tau_{\mathrm{lep}}\tau_{\mathrm{lep}}$ channel for signal Monte Carlo (red dotted line) and the data-based estimation of $Z \to \tau^+\tau^-$ background (black solid line) samples, normalized to unit area. Figure from [15].

describe the former, the *embedding* technique is used, where $Z \to \mu^+\mu^-$ events are selected in data and the reconstructed muons are replaced by simulated τ lepton decays. This means that the Z boson kinematics and all other event activity comes entirely from data. Fully data-driven techniques are used for the estimation of backgrounds from misidentified τ decay products as well, described in detail in [15].

2.2. Results

The signal is extracted by fitting the BDT shape with signal and background templates simultaneously in the six Signal Regions. Included in the fit are also nine Control Regions in order to better constrain the background normalizations. The post-fit BDT score distributions in the VBF category for each sub-channel are shown in Figure 2.

An excess of data events over the background prediction is observed in all three sub-channels. The fitted signal strength, $\mu = \sigma_{measured}/\sigma_{SM}$, is $1.43^{+0.31}_{-0.29}(\mathrm{stat.})^{+0.41}_{-0.30}(\mathrm{syst.})$ for $m_H = 125$ GeV; Figure 3 shows the best-fit values of μ in the individual channels. For the same mass, the observed (expected) probability p_0 of obtaining a result at least as signal-like if there actually is no signal is 2.0×10^{-5} (6.6×10^{-4}), corresponding to a 4.1σ (3.2σ) deviation from the background-only hypothesis – constituting direct evidence for $H \to \tau^+\tau^-$ decays.

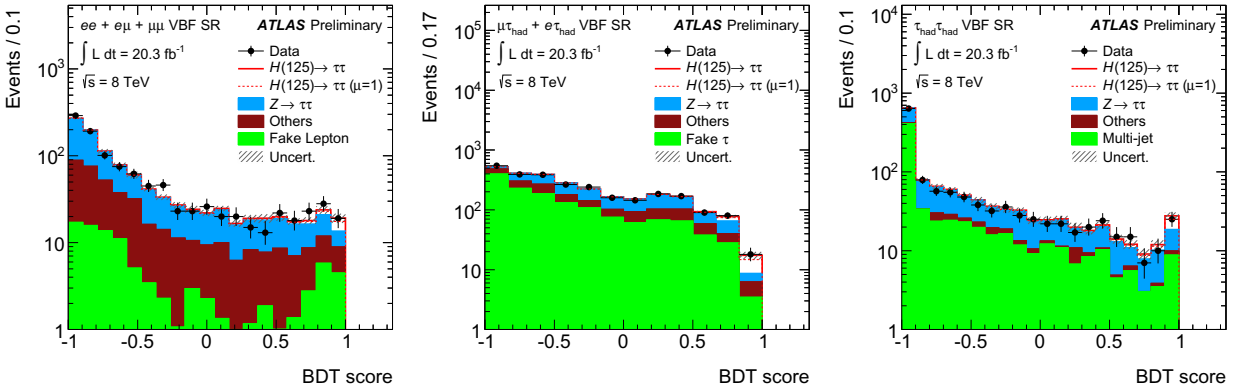

Figure 2: BDT distributions for the VBF category signal regions for the $\tau_{\text{lep}}\tau_{\text{lep}}$ (left), $\tau_{\text{lep}}\tau_{\text{had}}$ (centre) and $\tau_{\text{had}}\tau_{\text{had}}$ (right) sub-channels. The Higgs boson signal (for $m_H = 125$ GeV) is shown stacked, with $\mu = 1$ (dashed line) and $\mu = 1.4$ (solid line). The background predictions come from the global fit. The size of the statistical and normalization systematic uncertainties is indicated by the hashed band. Figures from [15].

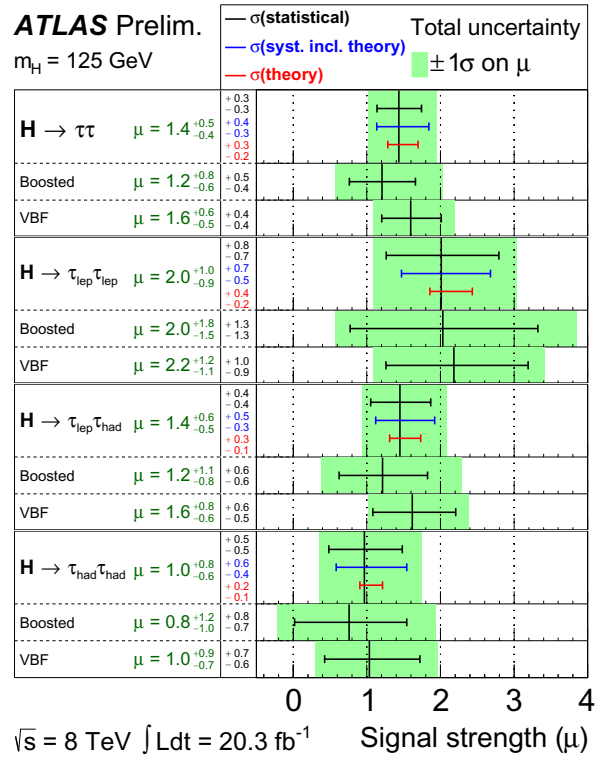

Figure 3: Summary of the best-fit value for the signal strength μ in the separate channels and in the combination. The shaded green band shows the total uncertainty ($\pm 1\sigma$). The individual contributions from the statistical uncertainty (top, black), the total (experimental and theoretical) systematic uncertainty (middle, blue), and the theory uncertainty on the signal cross section (bottom, red) are indicated with the error bars and printed in the central column. Figure from [15].

The most important uncertainty on the signal strength measurement is the statistical uncertainty of the data in the signal regions, followed by the theoretical systematic uncertainty on the differential cross section $d\sigma/dp_T^H$ for ggF production, the uncertainty on the normalization of the $Z \to \ell\ell$ and top quark backgrounds in $\tau_{\text{lep}}\tau_{\text{had}}$, and the uncertainty on the jet energy scale calibration.

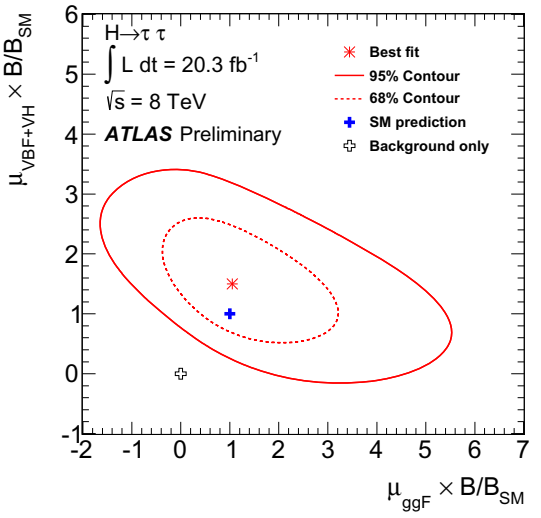

Figure 4: Likelihood contours in the $(\mu_{ggF} \times B/B_{SM}, \mu_{VBF+VH} \times B/B_{SM})$ plane, for $m_H = 125$ GeV. Figure from [15].

Figure 4 shows the results of a two-dimensional fit in the $(\mu_{ggF} \times B/B_{SM}, \mu_{VBF+VH} \times B/B_{SM})$ plane, where B and B_{SM} are the hypothesised and the SM branching ratios for $H \to \tau^+\tau^-$, and μ_{ggF} (μ_{VBF+VH}) the

signal strength for Higgs boson production proceeding through gluon fusion (VBF and associated production). The best-fit values are $\mu_{ggF} \times B/B_{SM} = 1.1^{+1.3}_{-1.0}$ and $\mu_{VBF+VH} \times B/B_{SM} = 1.6^{+0.8}_{-0.7}$.

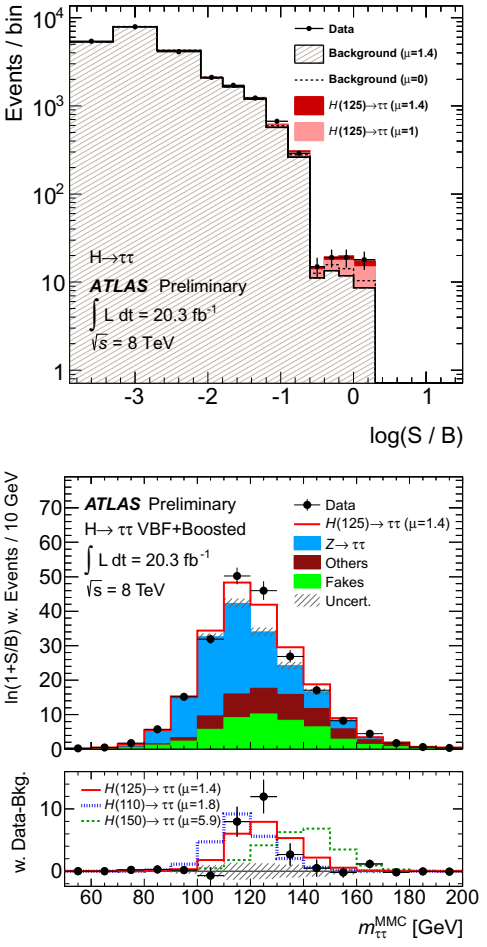

Figure 5: Top: Event yields, after the global fit, as a function of log(S/B), where S (signal yield) and B (background yield) are taken from each event's bin in the BDT. Bottom: Di-τ mass distribution where events are weighted by ln(1+S/B) for all channels, determined for each BDT bin separately. The bottom panel shows the difference between weighted data events and weighted background events (black points), compared to the weighted signal yields: the $m_H = 125$ GeV signal is shown with a solid red line, and, for comparison, the $m_H = 110$ GeV (blue) and $m_H = 150$ GeV (green) signals are also shown. Figures from [15].

To visualize the excess, Figure 5 (top) shows the fitted background and signal, as well as the observed data, for all signal region bins, ordered by their expected sensitivity. In Figure 5 (bottom), the weighted reconstructed di-τ mass distribution is presented. The distributions for the predicted excess in data over the background are shown for a SM Higgs boson mass hypotheses of $m_H = 110$ GeV and $m_H = 150$ GeV, as well as for $m_H = 125$ GeV, demonstrating the consistency of the excess with the latter case.

3. Higgs boson decays to muons

The $H \to \mu^+\mu^-$ channel presents a much better mass resolution compared to the tauonic decay, however its sensitivity is severely restricted by the low branching ratio of this decay for the Higgs boson in the SM. The search is performed by fitting the dimuon invariant mass distribution ($m_{\mu^+\mu^-}$) in the range of 110-160 GeV. This relatively wide range is chosen to allow determination of the background shape and normalization from the sidebands. Both the 7 TeV (4.5 fb^{-1}) and 8 TeV (20.3 fb^{-1}) datasets collected by the ATLAS experiment are used.

3.1. Analysis Description

Events are selected for the analysis if they contain exactly two isolated muons of opposite charge with a minimum p_T of 25 (15) GeV for the leading (sub-leading) muon. Additionally, a requirement on the missing transverse momentum being less than 80 GeV is also applied, reducing contamination from top quark pair production and diboson processes. Figure 6 shows the $m_{\mu^+\mu^-}$ distribution after this selection has been applied.

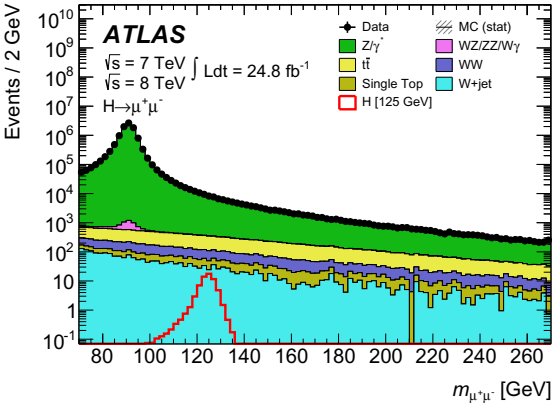

Figure 6: Distribution of $m_{\mu^+\mu^-}$ for events in 7 TeV and 8 TeV data passing the selection requirements described in the text. The red histogram indicates the expected signal for $m_H = 125$ GeV. Figure from [16].

Events passing this selection are then divided into seven mutually exclusive categories. Events with at least two jets, having an invariant dijet mass $m_{jj} >$

500 GeV, a pseudo-rapidity (η) separation of ($\eta_{j1} - \eta_{j2}$) > 3 and $\eta_{j1} \times \eta_{j2} < 0$, are placed in a VBF category. The remaining events are then split into categories according to the transverse momentum of their dimuon system ($p_{\mathrm{T}}^{\mu^+\mu^-}$): low ($<$ 15 GeV), medium (15 – 50 GeV) and high ($>$ 50 GeV). Events in each of these three categories are then further classified into a central (if both muons have $|\eta| < 1$) and a non-central (if one or both muons have $|\eta| > 1$) category. The reason for this final classification is that central muons yield a more precise momentum measurement, thereby producing a narrower invariant mass distribution and a higher overall sensitivity.

Analytic models are used to describe the signal and background $m_{\mu^+\mu^-}$ distributions, detailed in [16]. The signal is described by the sum of a Gaussian and a Crystal Ball function; the parameters of the model are obtained from fits to simulated SM Higgs boson samples, an example of which can be seen in Figure 7 (top). In the $p_{\mathrm{T}}^{\mu^+\mu^-}$ categories, the background is described using a Breit-Wigner convolved with a Gaussian function, added to an exponential divided by $1/m^3_{\mu^+\mu^-}$, while in the VBF category the background model is the product of a Breit-Wigner and an exponential function. In all cases, high-statistics samples of simulated background processes have been used to extensively validate the background model and to check against potential mismodelling bias. Figure 7 (bottom) shows the background model fit to data in one of the categories.

3.2. Results

The results of the search are obtained through a binned maximum likelihood fit to the observed $m_{\mu^+\mu^-}$ distribution in the 110-160 GeV range, using the sum of the signal and background model, simultaneously in all categories and for both 7 and 8 TeV datasets. No excess is seen over the background expectation and an exclusion limit can be placed on the $H \to \mu^+\mu^-$ signal strength, shown in Figure 8. For $m_H = 125.5$ GeV, the observed (expected) limit at 95% confidence level (CL) is 7.0 (7.2) times the SM prediction. For the same mass, assuming the SM production cross-section (allowed to vary within its uncertainties), a 95% CL upper limit on the branching ratio of $H \to \mu^+\mu^-$ can be placed at 1.5×10^{-3}.

4. Conclusions

A review of the latest ATLAS results in searches for Higgs boson decays to leptons has been presented. In the $H \to \tau^+\tau^-$ channel, an excess of a signal over the

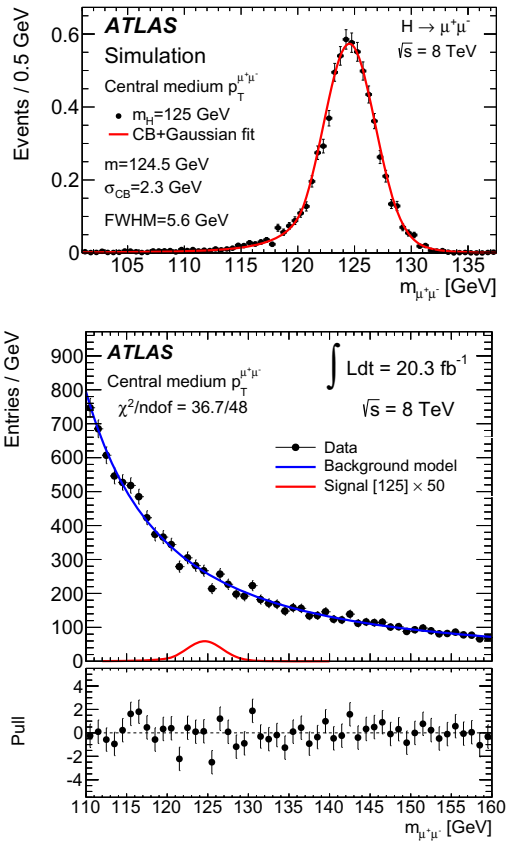

Figure 7: Top: The signal model fit to the $m_{\mu^+\mu^-}$ distribution for simulated Higgs boson events for $m_H = 125$ GeV in the central medium $p_{\mathrm{T}}^{\mu^+\mu^-}$ category. Bottom: The background model fit to the $m_{\mu^+\mu^-}$ distribution in data, for the same category. The statistical uncertainties are given for the data points. The expected signal is shown for $m_H = 125$ GeV and is scaled by a factor of 50. Figures from [16].

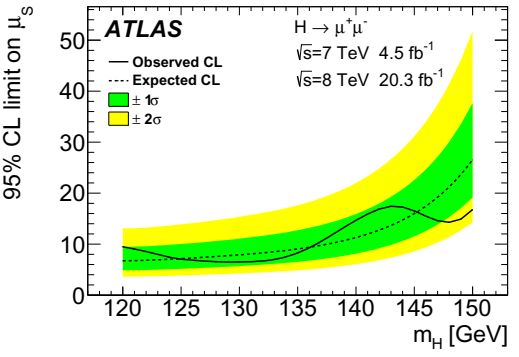

Figure 8: Observed (solid) and expected (dashed) 95% CL upper limits on the $H \to \mu^+\mu^-$ signal strength as a function of m_H. Figure from [16].

background has been observed, corresponding to an observed (expected) significance of 4.1σ (3.2σ) – constituting direct evidence for this decay. The measured signal strength is $\mu = 1.43^{+0.31}_{-0.29}$ (stat.) $^{+0.41}_{-0.30}$ (syst.), consistent with the SM expectation. In the $H \to \mu^+\mu^-$ search, an observed (expected) limit, at 95% CL, is placed on the signal strength at 7.0 (7.1) times the SM prediction, for $m_H = 125.5$ GeV. Assuming a SM production cross section, this corresponds to a limit on the branching ratio of $H \to \mu^+\mu^-$ of 1.5×10^{-3}. These results from the ATLAS experiment thus show that the Higgs boson does not couple universally to leptons, consistent with the SM prediction of Higgs boson couplings proportional to mass.

References

[1] ATLAS Collaboration, Observation of a new particle in the search for the Standard Model Higgs boson with the ATLAS detector at the LHC, Phys. Lett. B716 (2012) 1–29. doi:10.1016/j.physletb.2012.08.020.

[2] CMS Collaboration, Observation of a new boson at a mass of 125 GeV with the CMS experiment at the LHC, Phys. Lett. B716 (2012) 30–61. doi:10.1016/j.physletb.2012.08.021.

[3] L. Evans, P. Bryant (editors), LHC Machine, Vol. 3, 2008. doi:10.1088/1748-0221/3/08/S08001.

[4] CMS Collaboration, Observation of a new boson with mass near 125 GeV in pp collisions at $\sqrt{s}$ = 7 and 8 TeV, JHEP 1306 (2013) 081. doi:10.1007/JHEP06(2013)081.

[5] ATLAS Collaboration, Measurements of Higgs boson production and couplings in diboson final states with the ATLAS detector at the LHC, Phys. Lett. B726 (2013) 88–119. doi:10.1016/j.physletb.2013.08.010.

[6] ATLAS Collaboration, Evidence for the spin-0 nature of the Higgs boson using ATLAS data, Phys. Lett. B726 (2013) 120–144. doi:10.1016/j.physletb.2013.08.026.

[7] CMS Collaboration, Study of the Mass and Spin-Parity of the Higgs Boson Candidate Via Its Decays to Z Boson Pairs, Phys. Rev. Lett. 110 (2013) 081803. doi:10.1103/PhysRevLett.110.081803.

[8] F. Englert, R. Brout, Broken symmetry and the mass of gauge vector mesons, Phys. Rev. Lett. 13 (1964) 321. doi:10.1103/PhysRevLett.13.321.

[9] P. W. Higgs, Broken symmetries, massless particles and gauge fields, Phys. Lett. 12 (1964) 132. doi:10.1016/0031-9163(64)91136-9.

[10] P. W. Higgs, Broken symmetries and the masses of gauge bosons, Phys. Rev. Lett. 13 (1964) 508. doi:10.1103/PhysRevLett.13.508.

[11] G. S. Guralnik, C. R. Hagen, T. W. B. Kibble, Global conservation laws and massless particles, Phys. Rev. Lett. 13 (1964) 585. doi:10.1103/PhysRevLett.13.585.

[12] P. W. Higgs, Spontaneous symmetry breakdown without massless bosons, Phys. Rev. 145 (1966) 1156. doi:10.1103/PhysRev.145.1156.

[13] T. W. B. Kibble, Symmetry breaking in non-Abelian gauge theories, Phys. Rev. 155 (1967) 1554. doi:10.1103/PhysRev.155.1554.

[14] ATLAS Collaboration, The ATLAS Experiment at the CERN Large Hadron Collider, JINST 3 (2008) S08003. doi:10.1088/1748-0221/3/08/S08003.

[15] ATLAS Collaboration, Evidence for Higgs Boson Decays to the $\tau^+\tau^-$ Final State with the ATLAS Detector, ATLAS-CONF-2013-108, https://cds.cern.ch/record/1632191 (2013).

[16] ATLAS Collaboration, Search for the Standard Model Higgs boson decay to $\mu^+\mu^-$ with the ATLAS detector, Phys. Lett. B738 (2014) 68–86. doi:10.1016/j.physletb.2014.09.008.

[17] S. Dittmaier, et al., Handbook of LHC Higgs Cross Sections: 1. Inclusive Observables https://cds.cern.ch/record/1318996. doi:10.5170/CERN-2011-002.

[18] L. Breiman, J. Friedman, C. Stone, R. Olshen, Classification and Regression Trees, Chapman & Hall, 1984.

[19] J. H. Friedman, Stochastic gradient boosting, Comput.Stat.Data Anal. 38 (2002) 367–378. doi:10.1016/S0167-9473(01)00065-2.

[20] Y. Freund, R. E. Schapire, A decision-theoretic generalization of on-line learning and an application to boosting, J. Comput. Syst. Sci. 55 (1997) 119. doi:10.1006/jcss.1997.1504.

[21] A. Elagin, P. Murat, A. Pranko, A. Safonov, A New Mass Reconstruction Technique for Resonances Decaying to di-tau, Nucl. Instum. Meth. A654 (2011) 481–489. doi:10.1016/j.nima.2011.07.009.